PCCP

ROYAL SOCIETY OF CHEMISTRY

ARTICLE TYPE

Cite this: DOI: 10.1039/xxxxxxxxxx

Generalization of the Elastic Network model for the study of large conformational changes in biomolecules†

Adolfo B. Poma,*[a] Mai Suan Li,[a] and Panagiotis E. Theodorakis*[a]

Received Date
Accepted Date

DOI: 10.1039/xxxxxxxxxx

www.rsc.org/journalname

arXiv:1811.01191v1 [physics.bio-ph] 3 Nov 2018

The Elastic Network (EN) is a prime model that describes the long-time dynamics of biomolecules. However, the use of harmonic potentials renders this model insufficient for studying large conformational changes of proteins (*e.g.* stretching of proteins, folding and thermal unfolding). Here, we extend the capabilities of the EN model by using a harmonic approximation described by Lennard–Jones (LJ) interactions for far contacts and native contacts obtained from the standard overlap criterion as in the case of Gō-like models. While our model is validated against the EN model by reproducing the equilibrium properties for a number of proteins, we also show that the model is suitable for the study of large conformation changes by providing various examples. In particular, this is illustrated on the basis of pulling simulations that predict with high accuracy the experimental data on the rupture force of the studied proteins. Furthermore, in the case of DDFLN4 protein, our pulling simulations highlight the advantages of our model with respect to Gō-like approaches, where the latter fail to reproduce previous results obtained by all-atom simulations that predict an additional characteristic peak for this protein. In addition, folding simulations of small peptides yield different folding times for α-helix and β-hairpin, in agreement with experiment, in this way providing further opportunities for the application of our model in studying large conformational changes of proteins. In contrast to the EN model, our model is suitable for both normal mode analysis and molecular dynamics simulation. We anticipate that the proposed model will find applications in a broad range of problems in biology, including, among others, protein folding and thermal unfolding.

1 Introduction

One of the main goals in the computer simulation arena of biomolecules is to build the simplest yet computationally most efficient models able to reproduce accurately and predict faithfully dynamic and structural properties of proteins. A most prime example of this is the elastic network (EN) [1], which reproduces well the low-frequency motion (long-time dynamics) of proteins. The EN has been also employed for modelling other important biomolecules such as DNA [2], RNA [3,4], graphene sheet [5], and cellulose fibers [6], providing information on their equilibrium dynamics, the influence of the native-structure topology on their stability, the localization properties of protein fluctuations or the definition of protein domains [7]. Although a number of similar models have subsequently appeared in the literature and various improvements have been suggested [8–13], the EN still remains the standard model having attracted particular interest due to its simplicity and ability to provide realistic frequency data [7]. The use of EN model for studying processes that involve large conformational changes of proteins is a current challenge though, in practice due to the required numerical complexity. Therefore, several methodologies have been developed to tackle this problem. For example, certain approaches are based on the update of the connectivity or Kirchoff matrix during a linear interpolation between two known protein states [14–17]. However, this approximation fails when the two states are unknown or when one or both of these states are represented by an ensemble of equivalent configurations (*e.g.* unfolded state).

The EN model is based only on a single-parameter harmonic potential between residues that are represented in the model by the C_α atoms. In this model, the harmonic interaction is introduced when two residues overlap, *i.e.* the van der Waals radii augmented by a cutoff distance of any pairs of atoms belonging to different residues overlap (see Table 1). Here, the harmonic approximation of EN contacts models the interaction between C_α

[a] *Institute of Physics, Polish Academy of Sciences, Al. Lotników 32/46, 02-668 Warsaw, Poland; E-mail: poma@ifpan.edu.pl, panos@ifpan.edu.pl*

† Electronic Supplementary Information (ESI) available: Harmonic approximation for the Lennard–Jones potential. Pulling results for titin and sequence of transition states during pulling simulation. See DOI: 10.1039/cXCP00000x/

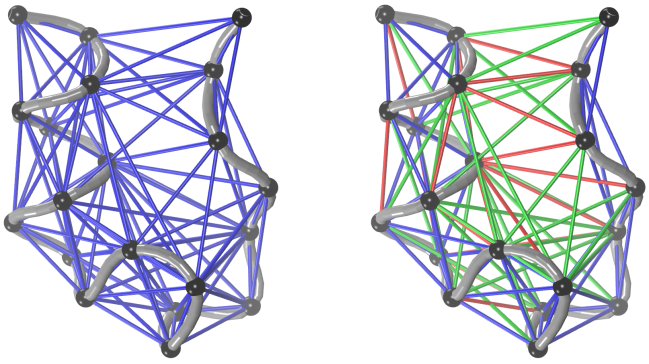


Fig. 1 Left panel shows the EN model for a tryptophan-cage motif (PDB ID: 1L2Y), the "unbreakable" harmonic EN contacts are shown in blue color. Right panel shows the GEN model, where a subset of the EN contacts are formulated as Gō contacts (in red) and far contacts by an effective harmonic term based on the LJ potential (in green). The EN and GEN models do not assume *a priori* C_α-backbone connectivity. Hence, the tube representation of the C_α backbone in grey serves only as a guide for the eye. Still, consecutive C_α atoms are connected by EN harmonic bonds, because they are within the cutoff distance of the EN model (see main text for further details).

atoms in the native state, such as the electrostatic and van der Waals interactions, as well as the covalent bonds along the backbone of C_α atoms (Fig. 1). On the one hand, the harmonic approximation is incompatible with the dissociation of native contacts for certain processes involving large conformational changes in biomolecules. On the other hand, some important advantages of the EN from the modeling point of view are avoiding: the use of computationally expensive simulations based on all-atom force-fields and the necessity of including *ad hoc* backbone stiffness in the model. The latter is generally implemented in coarse-grained models based on C_α atoms[18–20] to mimic the all-atom description of proteins, which is based on harmonic interactions used to maintain bonds and bond and dihedral angles. Technically, the EN model[1] is suitable for Normal Mode Analysis (NMA), which requires the calculation of the second-derivative (or Hessian) matrix. However, this step requires substantial computer memory and processing power to perform the matrix diagonalization, which becomes a severe bottleneck in the study of very large complexes. Moreover, one typically ignores molecular-interaction details[21] at this coarse-grain level of description, which is an approach that has been shown to work better in cases where the protein is packed uniformly[22]. While an initial energy-minimization step is needed to satisfy the harmonic pairs (*e.g.* steepest descent[23] and conjugate gradient[24] methods), this is not necessary for small systems[25].

Despite the aforementioned advantages of the EN, this model cannot be currently used for studying certain processes that involve large conformational changes of proteins apart from a few previous attempts that require *a priori* knowledge of the protein states[14–17], due to the presence of the harmonic bonds. In the following, we overcome this barrier and enhance the number of possible applications of the EN, for example, protein stretching[20,26–29], prediction of elastic properties[30] without the assumption of continuum theory[31], characterization of folding pathways[32] denaturation due to high temperature[33], pressure[34] and surfactants[35], as well as denaturation processes at interfaces (*e.g.* air–water and oil–water interfaces) based on simple CG potentials[36]. Here, we propose a model where harmonic interactions beyond the nearest neighbors (distance in sequence larger than three) are substituted by harmonic effective terms approximated by the Lennard–Jones (LJ) potential[37]. In addition, our model assumes LJ contacts obtained from a contact map based on the standard overlap criterion (Fig. 1)[38,39], namely, we determine native contacts based on the overlap (OV) of vdW radii of heavy atoms (N, C, C_α and O). For the determination of the contact map one considers each residue as a cluster of spheres. In this case, the radii of the spheres are equal to the van der Waals radii enhanced by a factor of about 25% (see Table 1). In addition, our model does not require bending- and dihedral-angle parameters along the Cα backbone in the native state. Our model is based only on a single parameter as the EN model does, but it enables the study of large-conformational changes in biomolecules due to the use of the contact map. In this respect, we anticipate that our work opens the door for the use of EN in a wider range of applications, for example, folding, thermal unfolding, denaturation of proteins at interfaces, *etc*.

In the following sections, we provide details about our model and methodologies. After validating the proposed model with the EN model for a number of proteins, we present various studies that involve large conformational changes of proteins highlighting model's advantages in comparison with the EN and Gō-like models.

2 Materials and Methods

2.1 Generalized elastic network model

In the case of EN, if any two heavy atoms belonging to different residues are within a distance $r_c = vdW_i + vdW_j + R_c$, then the two residues form an EN contact and a harmonic potential that connects the C_α positions of these residues is applied. R_c is simply a cutoff distance and vdW_i and vdW_j are the van der Waals radii of heavy atoms belonging to residues i and j (see Table 1). In this case, the harmonic potential has the form $V_h = C(r_{ij} - r_{ij}^0)^2$, where r_{ij}^0 is the distance between C_α atoms in the native structure of the protein and C is a constant indicating the strength of the harmonic potential. The energy scale associated to the EN model[1] is given by $\varepsilon_{EN} = CR_c^2$. In the case of our model, we use the same guideline for defining contacts due to EN. They contribute both to bonded and nonbonded energy of the Hamiltonian. The energy can be written as,

$$\mathscr{H} = \sum_{|i-j|<4} C(r_{ij} - r_{ij}^0)^2 + \sum_{|i-j|>3} \mathscr{U}_{ij}^{nb} \qquad (1)$$

The first term is the standard harmonic potential associated with the EN model while the second term is the nonbonded contribution, which enables large conformational changes in the protein. This second term is defined as follows:

This journal is © The Royal Society of Chemistry [year]

Table 1 List of vdW radii for heavy atoms used to determine the presence of the native contacts in proteins, sugars, and the sugar–protein complex. The third column refers to proteins. The values are taken from ref.[39]. The radii of the enlarged spheres are defined as the vdW radii multiplied by 1.24 to account for attraction[40].

No.	Atomic Group	vdW radius [Å]	enlarged radius [Å]
1	C_3H_0	1.61	2.00
2	C_3H_1	1.76	2.18
3	C_4H_1	1.88	2.33
4	C_4H_2	1.88	2.33
5	C_4H_3	1.88	2.33
6	N_3H_0	1.64	2.03
7	N_3H_1	1.64	2.03
8	N_3H_2	1.64	2.03
9	N_4H_3	1.64	2.03
10	O_1H_0	1.42	1.76
11	O_2H_1	1.46	1.81
12	S_2H_0	1.77	2.19
13	S_2H_1	1.77	2.19

$$\mathscr{U}_{ij}^{nb} = \begin{cases} U_{LJ}(\varepsilon_{cm}) & \text{if a native contact forms according to the OV criterion as in Gō-like models} \\ U_{LJ}(\varepsilon_{harm}) & \text{If a non-native contact forms according to the cutoff distance as in the EN model} \end{cases} \quad (2)$$

The native contacts found by the OV criterion are described by a Gō-like model[41,42] with LJ interactions ($U_{LJ}(\varepsilon_{cm})$). In addition, we use an effective-harmonic term based on the LJ potential [$U_{LJ}(\varepsilon_{harm})$] for contacts between residues with a distance in sequence larger than three. The LJ potential reads

$$U_{LJ}(\varepsilon_{ij}) = 4\varepsilon_{ij}\left[\left(\frac{\sigma_{ij}}{r_{ij}}\right)^{12} - \left(\frac{\sigma_{ij}}{r_{ij}}\right)^{6}\right], \quad (3)$$

where r_{ij} is the distance between any pair of i and j C_α atoms in the system. The relation between the effective harmonic term and the strength of the LJ potential ε_{ij} is simply described by the formula[37]: $\varepsilon_{ij} = \varepsilon_{harm}$, where $\varepsilon_{harm} = C\sigma_{ij}^2 36^{-1}(2^{2/3})$ (see SI), $\sigma_{ij} = 2^{-1/6} r_{ij}^0$. Hence, one infers about the ε_{harm} from C and r_{ij}^0. In addition, we include contacts by using a contact map based on the standard overlap criterion[38,39]. The latter contacts are represented by LJ potentials $U_{LJ}(\varepsilon_{cm})$[43,44]. In this case, the strength of interaction is independent of the distance and equal to $\varepsilon_{ij} = \varepsilon_{cm}$ for any pair of residues in contact, where ε_{cm} is the unit of energy, and $\sigma_{ij} = 2^{-1/6} r_{ij}^0$. Here, the subindex "cm" denotes the "contact map" obtained by the overlap criterion. Moreover, the latter contacts apply only for residues at a sequential distance larger than three. If a native contact coincides with a harmonic effective contact, then the native contact [$U_{LJ}(\varepsilon_{cm})$] remains and the harmonic contact [$U_{LJ}(\varepsilon_{harm})$] is removed. An important characteristic of the model is the proper balance of the energy scales assigned between contacts for the C_α backbone and those that represent the non-bonded contributions. In particular, there are three energy scales: the EN-type interactions (ε_{EN}), the native (ε_{cm}) and the effective harmonic-type interactions (ε_{harm}). $\varepsilon_{EN} = CR_c^2$, which corresponds to 12.250 kJmol^{-1} for $R_c = 0.35$ nm, and $\varepsilon_{cm} = 6.276$ kJmol^{-1}, which reflects the strength of hydrogen bond in proteins[37]. ε_{harm} is about 2.0 kJmol^{-1}. Henceforth, we will simply refer to our model as Generalized Elastic Network (GEN) model. We have also investigated other possibilities, such as excluding the effective harmonic interactions $U_{LJ}(\varepsilon_{harm})$ and substituting all effective harmonic terms with standard LJ potentials ($\varepsilon_{ij} = \varepsilon_{cm}$, "M1" model) or eliminating all contacts beyond 1–4 [$U_{LJ}(\varepsilon_{harm})$] and keeping only the native contacts [$U_{LJ}(\varepsilon_{cm})$] based on the overlap criterion ("M2" model) . Finally, we have also considered the case that we have all EN harmonic bonds irrespective of the sequential distance between residues as in the standard EN model, but those contacts that coincide with the native contacts derived from the overlap criterion will be substituted by LJ potentials $U_{LJ}(\varepsilon_{cm})$ resulting in what we will simply refer to as the "M3" model. In the following, we will discuss these models for the sake of comparison with the GEN and EN models on the basis of the different number of harmonic, effective harmonic and Gō contacts (see Table 2).

2.2 Normal mode analysis and pulling simulations

We used the GROMACS package[45–48] to perform standard Normal Mode Analysis (NMA)[7]. The output of NMA is independent (normal) modes (harmonic motions) characterized by an eigenvalue (characteristic frequency). Each normal mode acts as a simple harmonic oscillator of a concerted motion of atoms without moving the center of mass with all atoms passing through their equilibrium position at the same time. Moreover, normal modes resonate independently and can be obtained directly by data obtained from vibrational spectroscopy. In practice, the normal modes are the eigenvectors of the Hessian matrix, which represents the force constants between every possible pair of residues in the system in all directions of the Cartesian coordinate system.

The mean square fluctuations of the C_α atoms are calculated

from the normal modes as follows:

$$\langle \Delta r_j^2 \rangle = k_B T \sum_i \frac{|\vec{a}_{ij}|^2}{\omega_i^2}, \quad (4)$$

here, $\vec{a}_{ij}$ is the vector of the projections of the i-th eigenvector of the normal modes set with frequency ω_i on the Cartesian components of the displacement vector for the j-th C_α atom, k_B is the Boltzmann constant, and, T, the reference temperature. The B-factor related to the expected residue fluctuations is calculated by the following relation

$$B_j = \frac{8\pi^2}{3} \langle \Delta r_j^2 \rangle. \quad (5)$$

To perform the protein stretching, we used Molecular Dynamics (MD) simulation in the NVT ensemble. The time step was 0.01 ps and the protein was pulled along the end-to-end vector connecting the C_α-atoms from the N- and C-termini and the reaction coordinate is the displacement of the pulling spring. Moreover, additional beads have been attached to those C_α-atoms with the spring constant being 37.6 kJ mol^{-1} nm^{-2}, which is a typical value of the Atomic Force Microscopy (AFM) cantilever stiffness in protein stretching studies[49]. Each system was pulled over the course of 10^7 ps with a velocity of 10^{-2} m/s. Although this value is still far from the experimental value of cantilever velocity[50] ($\sim 10^{-6}$ m/s), it gives comparable results with experiments showing the intrinsic speedup associated to the smoothing of the potential energy landscape, which is typical for coarse-grain methods.

3 Results and Discussion

In this section, we first validate the GEN model in terms of B-factors by comparing with data obtained from the EN model. Then, using this model we have performed stretching and folding simulations, in this way providing two illustrative examples of large conformation changes in proteins.

3.1 Validation of the GEN model

To validate our model, we have calculated the B-factors for several target proteins by using NMA[51], which are proportional to the mean square fluctuations of atom positions. We juxtaposed our results with those of Tirion[1], which were also obtained by using the same EN approach (Fig. 2). The results shown in Fig. 2 were obtained for a cutoff distance of $R_c = 0.35$ nm, but, for other models considered in this study, we have also investigated different cutoffs, namely, R_c = 0.2 - 0.85 nm. In our case, the best correlation was obtained for R_c =0.35 nm. Our data manifests an excellent agreement with the EN model showing that the GEN model reproduces closely the properties of the EN, which we have also confirmed for all proteins discussed in ref.[1] providing a theoretical validation of the GEN model in the case of the chosen set of proteins. Another EN model, the so-called Gaussian Network model (GNM)[8,9], is able to reproduce closer the experimental results of B-factor related to larger protein complexes. However, this may not be the case for atomic fluctuations derived from all-atom simulation[52]. Moreover, the GNM cannot be used in simulation and, therefore, the one-to-one correspondence with short-time atomic fluctuations is not conceived in this formalism. In addition, this model introduces additional concepts from the elastic theory of random polymer network[53] and it is found to be more appropriate to reproduce available experimental fluctuation data reported by the B-factors in the case of G-actine. Yet, even models based on this assumption are not reliable for describing large conformational changes as they rely by construction on the "unbreakable" harmonic bonds.

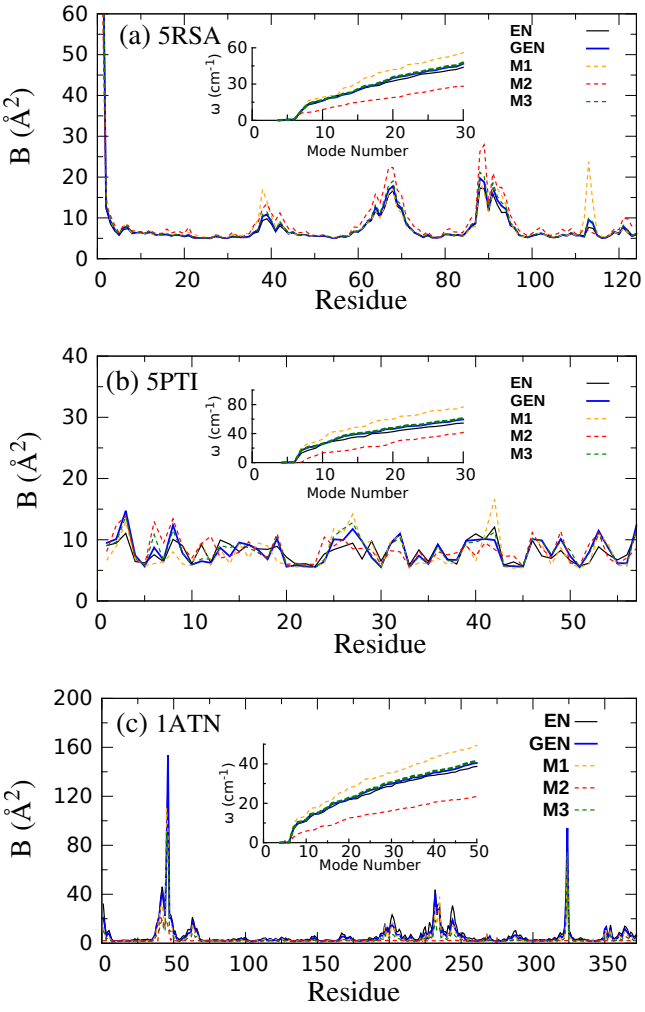


Fig. 2 The B-factors for the lowest 30 modes for the proteins with PDB ID: 5RSA (Ribonuclease-A, a) , 5PTI (Bovine Pacreatic Trypsin Inhibitor, b), and 1ATN (G-actine, c). The results obtained from different models are illustrated as indicated. Here, R_c =0.35 nm. Insets show the frequency ω (cm^{-1}) for the lowest 30 modes.

To further validate the GEN model, we have compared it with the standard EN and other possible versions of a breakable EN model (M1, M2 and M3) for a number of different protein structures determined by X-Ray diffraction and within 1-2 Å of resolution. For this purpose, we performed extensive tests on the following proteins: The first one is about 124 residues (PDB ID: 5RSA) and corresponds to ribonuclease A[55], the second one is obtained from the bovine pancreatic trypsin inhibitor[56] with a length of 58 residues (PDB ID: 5PTI), and the last one corresponds to a muscle

This journal is © The Royal Society of Chemistry [year]

Table 2 Total number of bonds/contacts for different models as indicated. Here, the columns are as follows: "EN" indicates the number of EN bonds, "cm" the number of native contacts by using the contact map (overlap criterion), and the "Eff. Harm. (LJ)" indicates the number of effective-harmonic contacts. R_c =0.35 nm.

	PDB ID:1AOH			PDB ID:1TIT		
Nr. of bonds/contacts / Model	EN	cm	Eff. Harm. (LJ)	EN	cm	Eff. Harm. (LJ)
Elastic Network	1131	–	–	632	–	–
GEN	352	349	430	203	156	273
M1	352	779	–	203	429	–
M2	352	349	–	203	156	–
M3	782	349	–	476	156	–

protein (G-actine)[57] with 373 residues ((PDB ID: 1ATN). The first two protein chains are made by helices and beta-strands while the last chain is folded so as to form two large domains joined by a narrow neck region. These two domains are partly held together by salt bridges and hydrogen bonds provided by a nucleotide that stabilizes the two domains. Our NMA results are presented in Fig. 2 along with their corresponding frequency data. Clearly, the GEN model exhibits the best agreement with the EN, again indicating the very good approximation of our harmonic terms with appropriate effective LJ interactions and the small influence of the native LJ contacts in the model. We have also checked a number of additional proteins and we have found consistent results and a similar agreement between the GEN and the EN models. Moreover, the M3 model, which has undergone a small modification by including the native LJ contacts in the EN, exhibits obviously almost absolute agreement with the EN, whereas the M1 and M2 models show considerable deviation from the EN, due to the lack of a large number of harmonic or effective-harmonic interactions $[U_{\rm LJ}(\varepsilon_{\rm harm})]$ (see Table 2). This shows that the $U_{\rm LJ}(\varepsilon_{\rm cm})$ terms are not enough to preserve the structure and properties of the targeted proteins without assuming extra terms that contribute to backbone stiffness (*e.g.* bond and dihedral angles). Moreover, the latter terms require tuning, as in the case of Gō-like models. For a comparison of 64 different Gō models, see Ref.[40].

3.2 Pullling simulations

As our aim here is to propose an as simple and accurate as possible model for studying mechanical unfolding of proteins, we have carried out pulling simulations in the same manner as in the case of single molecule studies performed with AFM[26,49]. We used implicit solvent conditions similar to ref.[58]. Overall, the correct redistribution of contacts between the above three categories (see Table 2) results in the excellent agreement of our simulations results (GEN model) with the experimental maximum pulling force, $F_{\rm max}$, in pulling simulations as is shown here for two examples, cohesin (PDB ID: 1AOH) (Fig. 3) and I27 domain of titin (PDB ID: 1TIT) (see Fig. S1 in SI). The temperature during pulling simulations is $0.3\varepsilon_{\rm cm}/k_{\rm B}$. The early unfolding scenario at the experimental pulling speed, which gives rise to the assessment of the mechanical properties of proteins, is difficult to achieve by using all-atom simulations, because the time-scale involved is too short for stretching proteins in the case of all-atom methods. In particular, the typical speed used to stretch proteins in all-atom simulations is nowadays of the order of 10^{-2} nm/ps[59] and the experimental cantilever speed is around 10^{-9} nm/ps[49]. In this regard, the CG nature of our approach can be used to study a range of speeds much closer to the experimental conditions in comparison with all-atom models.

Multiple proteins are linked sequentially and one can typically observe a number of corresponding peaks, which signal the full unfolding of individual protein modules. Due to the space resolution, intermediate unfolding states are not detected in AFM experiments[60]. However, by using CG models one can usually access these intermediate states with a better resolution and assign to each of them a force peak[20]. The largest of these force peaks, $F_{\rm max}$, defines the characteristic unfolding force for the whole protein domain.

The GEN model is the best to reproduce the experimental rupture force for cohesin and the I27 domain of titin (Fig. 3). In particular, the maximum force is 480±14 and 204±30 pN for 1AOH, and 1TIT, respectively (see SI). The M2 model provided a much lower force peak, while a much higher one was observed in the case of the M1 model. This can be explained in terms of the number of contacts associated with the LJ interactions (see Fig. 3, bottom panel), which in the case of M2 model appears to be smaller, but in the case of M1 is much larger (Table 2). In addition, in the case of M3 and EN models there is no peak due to the presence of the harmonic bonds between the C_α atoms that prevent the unfolding even at very large stretching forces. The unfolding pathway for 1AOH protein has been previously characterized by a Gō-like model[61] and experiment[62]. It is known that the detachment of $\beta_1(6-15)$ from $\beta_9(136-147)$ domains occurs at the same position of the maximum force in the F-d plot. We have carried out the analysis of native contacts between pairs of β-strands which are responsible for stabilizing the protein (see SI). Our results capture the sequential detachment of the secondary structures that give rise to the largest force peak. Our observation agrees well with the breaking of native contacts between β_1 and β_9 strands. The characterization of the unfolding pathway for titin also agrees with the experimental results[63,64] and is shown in SI. Moreover, proteins do not show any spurious effects with respect to their structure (*e.g.* local aggregation) during the stretching due to the presence of harmonic bonds in the structure for our GEN model. We have further confirmed our conclusions by investigating a number of different proteins.

The mechanostability of the DDFLN4 protein (with PDB ID: 1KSR) has been studied experimentally[65,66] and theoretically

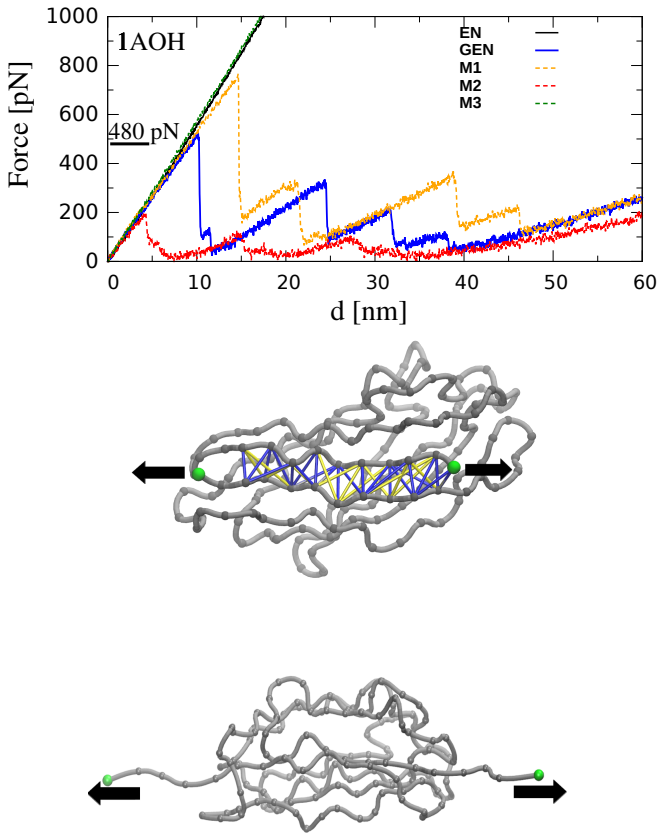


Fig. 3 Top panel shows the plot of force vs. cantilever displacement, d, for the type I cohesin domain (PDB ID: 1AOH). Also, the experimental value for the maximum force, which is 480±14 pN[54] in the case of 1AOH is indicated by a horizontal line. The bottom panel shows two snapshots at d = 0 nm and d = 10 nm. In the middle, we highlight the contacts responsible for the first peak (in blue) in GEN model and the additional yellow contacts that are present in the M1 model. We have performed a similar analysis for the I27 domain of titin (see SI).

with all-atom simulation by Kouza *et al.*.[69]. In experiment, two peaks were observed in the force–displacement curve: one was located at $d = 11$ nm and another one at 22 nm. Here, we tested the performance of the GEN model against a standard Gō-like model[68] for this protein. The Gō-like model captures the first experimental peak approximately at $d = 13$ nm, but it misses the second peak (see Figure 4). This is due to the lack of additional far distance contacts, which are only included by the GEN model (in GEN model these are treated by the harmonic approximation). In this regard, the GEN model performs better than the Gō-like model as it reproduces both experimental peaks. Moreover, the GEN model is as good as the all-atom model[69] in predicting mechanical unfolding intermediates because both models provide three peaks at nearly the same positions. Note that in our CG simulations we obtained an earlier force peak at $d = 4$ nm, which is consistent with all-atom simulation[69]. However, this peak has not been detected in experiment.

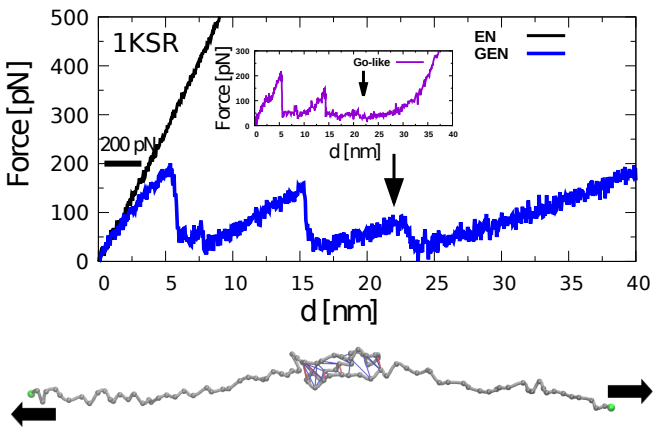


Fig. 4 Top panel shows the force–displacement profiles for domain 4 of the DDFLN4 protein. The results were obtained by using the GEN model (blue line), the EN model (black line) and the Gō model (inset) for pulling speed v=5×10^{-4} nm/τ, where τ is approximately 1ns. Results were averaged over 40 trajectories. Arrows refer to positions of the second peak at $d = 22$ nm, which is expected to be the same as in experiments[65,66]. Bottom panel illustrates a simulation snapshot for $d = 22$ nm, where the contacts that stabilize the structures are in blue (Gō-like) and in red (harmonic). The N- and C- termini beads are shown in green and the pulling direction is denoted by arrows. The data points for the Gō-like model were extracted by using g3data software[67] from ref. [68].

3.3 Folding simulation of small peptides

We are presenting here the folding process of two, well documented in the literature, small peptides, namely, an α-helix comprising the sequence segment 70–83 of the protein HPr from Escherichia coli (PDB ID: 1HDN[70] with 85 residues in total) and a β-hairpin (residues 41–56 of the immunoglobulin binding domain of streptococcal protein G with PDB ID: 1GB1[71] and 56 residues in total). Initial configurations for MD simulation are unfolded conformations without any Gō-like or effective harmonic contacts. According to a standard criterion that is commonly used in the case of Gō-like models, the Gō-like contacts are present in the structure when the actual distance between two C_α atoms is smaller than $1.5\sigma_{ij}$, where r_{ij}^0 is the distance between two C_α atoms that form a contact in the native conformation. Unfolded structures were obtained by heating up the system at 500 K without water and making sure that no native contacts are present in the protein structure by using the above criterion based on the distance between the C_α atoms in the native structure. In this way, we produced initial configurations for 50 statistically independent MD trajectories of length 200 τ at 300 K. Figure 5 shows the convergence of the total number of contacts towards the folded structure.

The GEN model and two of its variants (M1 and M2) allow for the study of protein folding, whereas the EN model apparently is not suitable for folding studies, due to the presence of the harmonic bonds. Our results and typical snapshots of unfolded and well-folded (native) structures are presented in Figure 5. In the case of the α-helix, the folding did occur in all independent trajectories, whereas about 5% of the trajectories in the case of β-hairpin did not reach the native structure within

This journal is © The Royal Society of Chemistry [year]

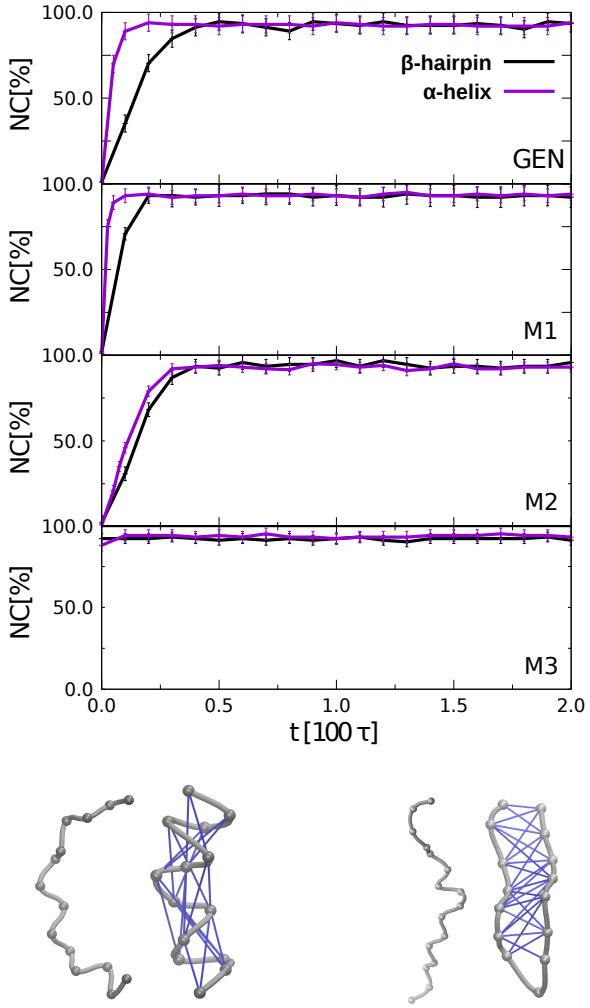


Fig. 5 Folding of two small peptides, a β-hairpin and an α-helix. Plots show the percentage of Gō-like and harmonic contacts present at a certain time during the folding process for each case and breakable model. Top panel for GEN model, middle panels for M1 model and M2 and bottom panel for M3 model, as indicated. A typical folding time for the α-helix is about 10 τ, while for the β-hairpin it is about 70 τ in the GEN model. Snapshots indicate examples of an unfolded state at the beginning of the simulation and a final folded (native) structure for each peptide. The C_α atoms are represented by grey color. Native and harmonic contacts are described by solid blue lines.

the time scale of the simulation. Assuming that the time unit τ=1 ns, we obtained the folding times for β-hairpin and α-helix equal to t^{β}_{fold}= 70 ns and t^{α}_{fold}= 10 ns , respectively. According to the temperature-jump fluorescence experiment by Munoz *et al.*[72], $t^{\beta}_{fold} \approx 6\mu$s. Since the folding time of α-helix is about 0.7 μs[73] the experimental ratio $t^{\beta}_{fold}/t^{\alpha}_{fold} \approx 9$, which is close to the value of 7, which was obtained from our simulations. In this regard, the other models underestimate the ratio. For instance, M1 and M2 give approximately 2 and 1.3, respectively. Moreover, the M3 model does not capture any distinction between both peptides. This is due to the presence of the harmonic contacts that place the unfolded state in a very high energy state. This induces a rapid process towards the folded state just after energy minimization. Still, the absolute folding time in GEN is much shorter than the real time, due to the coarse-graining, while all-atom simulations from different groups have predicted values in the range 1–7 μs[74–76]. The fact that folding of the α-helix is about seven times faster than the folding of the β-hairpin in the GEN model is also in agreement with our previous study[20], whereas M1 and M2 lead to a shorter time scale separation.

4 Conclusions

In conclusion, this work presents a simple and apparently accurate model based on the EN approach for studying large conformational changes in proteins. Here, we have shown that the GEN model, despite its simplicity, maintains a close match with the EN, while it reproduces with high accuracy the maximum force in AFM-pulling experiments and the folding time scales of peptides. On the one hand, there are several limitations in modeling proteins by CG approaches in particular due to the lack of details (*e.g.,* solvent effect, amino acid specificity, *etc.*) and thus we do not expect to capture all possible effects that stabilize protein complexes. However, our model handles native interactions with simplicity (Gō-like potentials), which is crucial for enabling conformational changes. Moreover, the effective harmonic interactions described by LJ potentials and the native Gō-like potentials prevent the steric clashes during the studies carried out in the present work. However, more sophisticated functional forms of non-native interactions could be included *a posteriori* and their effect may be relevant in other applications. The GEN model has enabled the study of protein folding confirming the timescale separation (about seven-fold difference in folding time between the α-helix and the β-hairpin). On the other hand, our model uses a reduced number of parameters in comparison with any structured-based CG model that enables large conformational studies, while its foundation is based on the simple EN model with no assumptions about backbone connectivity. As we have shown, the GEN model provides the same number of peaks in the force–displacement profile as observed in the case of the all-atom models for the DDFLN4 protein. This result highlights the advantage of our model over standard Go-like models. In perspective, one can interface the GEN model with knowledge-based and free-energy derived potentials for the study of protein aggregation phenomena. It could also be used to study denaturation phenomena, for example, due to large changes in temperature or pressure. Such and other phenomena could possibly be described by our simple EN-type model and it would be interesting to check in the future the prediction power of GEN for different protein systems.

Acknowledgements

This research has been supported by the National Science Centre, Poland, under grant No. 2015/19/P/ST3/03541, No. 2015/19/B/ST4/02721, and No. 2017/26/D/NZ1/00466. This project has received funding from the European Union's Horizon 2020 research and innovation programme under the Marie Skłodowska–Curie grant agreement No. 665778. This research was supported in part by PLGrid Infrastructure.

References

1 M. M. Tirion, *Phys. Rev. Lett.*, 1996, **77**, 1905–1908.

2 P. Setny and M. Zacharias, *J. Chem. Theory Comput.*, 2013, **9**, 5460–5470.

3 M. T. Zimmermann and R. L. Jernigan, *RNA*, 2014, **20**, 792–804.

4 G. Pinamonti, S. Bottaro, C. Micheletti and G. Bussi, *Nucleic Acids Res.*, 2015, **43**, 7260–7269.

5 M. H. Kim, D. Kim, J. B. Choi and M. K. Kim, *Phys. Chem. Chem. Phys.*, 2014, **16**, 15263–15271.

6 D. C. Glass, K. Moritsugu, X. Cheng and J. C. Smith, *Biomacromolecules*, 2012, **13**, 2634–2644.

7 Q. Cui and I. Bahar, *Normal Mode Analysis. Theory and applications to biological and chemical systems.*, Chapman & Hall/CRC, 2006.

8 I. Bahar, A. R. Atilgan and B. Erman, *Fold. Design*, 1997, **2**, 173–181.

9 T. Haliloglu, I. Bahar and B. Erman, *Phys. Rev. Lett.*, 1997, **79**, 3090.

10 K. Hinsen, *Proteins*, 1998, **33**, 417–429.

11 A. Hinsen, K. Thomas and M. Field, *Proteins*, 1999, **34**, 369–382.

12 A. R. Atilgan, S. R. Durell, R. L. Jernigan, M. C. Demirel, O. Keskin and I. Bahar, *Biophys. J.*, 2001, **80**, 505–515.

13 F. Tama and Y.-H. Sanejouand, *Protein Eng.*, 2001, **14**, 1.

14 M. K. Kim, R. L. Jernigan and G. S. Chirikjian, *Biophys. J.*, 2002, **83**, 1620–1630.

15 Y. Feng, L. Yang, A. Kloczkowski and R. L. Jernigan, *Proteins: Struct., Funct., Bioinf.*, 2009, **77**, 551–558.

16 A. Das, M. Gur, M. H. Cheng, S. Jo, I. Bahar and B. Roux, *PLOS comput. Biol.*, 2014, **10**, e1003521.

17 M. Tekpinar and W. Zheng, *Proteins: Struct., Funct., Bioinf.*, 2010, **78**, 2469–2481.

18 C. Clementi, H. Nymeyer and J. N. Onuchic, *J. Mol. Biol.*, 2000, **298**, 937–953.

19 J. Karanicolas and C. L. Brooks, *Protein Sci.*, 2002, **11**, 2351–2361.

20 A. B. Poma, M. Cieplak and P. E. Theodorakis, *J. Chem. Theory Comput.*, 2017, **13**, 1366–1374.

21 A. Van Wynsberghe, G. Li and Q. Cui, *Biochemistry*, 2004, **43**, 13083–13096.

22 Z. Bagci, A. Kloczkowski, R. L. Jernigan and I. Bahar, *Proteins: Struct., Funct., Bioinf.*, 2003, **53**, 56–67.

23 R. Fletcher and M. J. Powell, *Comput. J.*, 1963, **6**, 163–168.

24 D. S. Kershaw, *J. Comput. Phys.*, 1978, **26**, 43–65.

25 X. Periole, M. Cavalli, S.-J. Marrink and M. A. Ceruso, *J. Chem. Theory Comput.*, 2009, **5**, 2531–2543.

26 M. Rief, M. Gautel, F. Oesterhelt, J. M. Fernandez and H. E. Gaub, *Science*, 1997, **276**, 1109–1112.

27 M. S. Kellermayer, S. B. Smith, H. L. Granzier and C. Bustamante, *Science*, 1997, **276**, 1112–1116.

28 J. Sułkowska, A. Kloczkowski, T. Sen, M. Cieplak and R. Jernigan, *Proteins*, 2008, **71**, 45–60.

29 S. Kumar and M. S. Li, *Phys. Rep.*, 2010, **486**, 1 – 74.

30 N. Becker, E. Oroudjev, S. Mutz, J. P. Cleveland, P. K. Hansma, C. Y. Hayashi, D. E. Makarov and H. G. Hansma, *Nat. Mater.*, 2003, **2**, 278–283.

31 L. D. Landau and E. Lifshitz, *Course of Theoretical Physics*, 1986, **3**, 109.

32 S. E. Jackson, *Fold. Des.*, 1998, **3**, R81–R91.

33 S. Benjwal, S. Verma, K.-H. Röhm and O. Gursky, *Protein Sci.*, 2006, **15**, 635–639.

34 N. Hillson, J. N. Onuchic and A. E. García, *Proc. Natl. Acad. Sci. U.S.A.*, 1999, **96**, 14848–14853.

35 D. E. Otzen, *Biophys. J.*, 2002, **83**, 2219–2230.

36 Y. Zhao and M. Cieplak, *Phys. Chem. Chem. Phys.*, 2017.

37 A. Poma, M. Chwastyk and M. Cieplak, *J. Phys. Chem. B*, 2015, **119**, 12028–12041.

38 M. Cieplak and T. X. Hoang, *Biophys. J.*, 2003, **84**, 475–488.

39 J. Tsai, R. Taylor, C. Chothia and M. Gerstein, *J. Mol. Biol.*, 1999, **290**, 253–66.

40 J. I. Sulkowska and M. Cieplak, *Biophys. J.*, 2008, **95**, 3174–91.

41 N. Gō and H. Taketomi, *Proc. Natl. Acad. Sci. U.S.A.*, 1978, **75**, 559–563.

42 N. Gō and H. Abe, *Biopolymers*, 1981, **20**, 991–1011.

43 T. X. Hoang and M. Cieplak, *J. Chem. Phys.*, 2000, **113**, 8319–8328.

44 J. I. Sułkowska and M. Cieplak, *J. Phys. Condens. Matter*, 2007, **19**, year.

45 H. Berendsen, D. van der Spoel and R. van Drunen, *Comput. Phys. Commun.*, 1995, **91**, 43–56.

46 D. van der Spoel, E. Lindahl, B. Hess, G. Groenhof, A. Mark and H. Berendsen, *J. Comput. Chem.*, 2005, **26**, 1701–1718.

47 B. Hess, C. Kutzner, D. van der Spoel and E. Lindahl, *J. Chem. Theory Comput.*, 2008, **4**, 435–447.

48 S. Pronk, S. Páll, R. Schulz, P. Larsson, P. Bjelkmar, R. Apostolov, M. Shirts, J. Smith, P. Kasson, D. van der Spoel, B. Hess and E. Lindahl, *Bioinformatics*, 2013, **29**, 845–854.

49 M. Carrion-Vazquez, A. F. Oberhauser, S. B. Fowler, P. E. Marszalek, S. E. Broedel, J. Clarke and J. M. Fernandez, *Proc. Natl. Acad. Sci. U.S.A.*, 1999, **96**, 3694–3699.

50 P. E. Marszalek, H. Lu, H. Li, M. Carrion-Vazquez, A. F. Oberhauser, K. Schulten and J. M. Fernandez, *Nature*, 1999, **402**, 100–103.

51 I. Bahar and A. J. Rader, *Curr. Opin. Struct. Biol.*, 2005, **15**, 586–592.

52 E. Fuglebakk, N. Reuter and H. K, *J. Chem. Theory Comput.*, 2013, **9**, 5618–5628.

53 P. Flory, *Proc. R. Soc. Lond.*, 1976, **351**, 351–380.

54 A. Valbuena, J. Oroz, R. Hervás, A. M. Vera, D. Rodríguez, M. Menéndez, J. I. Sulkowska, M. Cieplak and M. Carrión-Vázquez, *Proc. Natl. Acad. Sci. U.S.A.*, 2009, **106**, 13791–13796.

55 A. Wlodawer, N. Borkakoti, D. Moss and B. Howlin, *Acta Crystallogr. B*, 1986, **42**, 379–387.

56 A. Wlodawer, J. Walter, R. Huber and L. Sjölin, *J. Mol. Biol.*,

This journal is © The Royal Society of Chemistry [year]

1984, **180**, 301–329.
57 W. Kabsch, H. G. Mannherz, D. Suck, E. F. Pai and K. C. Holmes, *Nature*, 1990, **347**, 37.
58 M. Cieplak, T. X. Hoang and M. O. Robbins, *Proteins: Struct., Funct., Genet.*, 2002, **49**, 114–124.
59 M. Sotomayor and K. Schulten, *Science*, 2007, **316**, 1144–1148.
60 P. E. Marszalek, H. Lu, H. Li, M. Carrion-Vazquez, A. F. Oberhauser, K. Schulten and J. M. Fernandez, *Nature*, 1999, **402**, 100–103.
61 M. Wojciechowski, P. Szymczak, M. Carrión-Vázquez and M. Cieplak, *Biophys. J.*, 2014, **107**, 1661–1668.
62 A. Valbuena, J. Oroz, R. Hervás, A. M. Vera, D. Rodríguez, M. Menéndez, J. I. Sulkowska, M. Cieplak and M. Carrión-Vázquez, *Proc. Natl. Acad. Sci. U.S.A.*, 2009, **106**, 13791–13796.
63 S. B. Fowler, R. B. Best, J. L. T. Herrera, T. J. Rutherford, A. Steward, E. Paci, M. Karplus and J. Clarke, *J. Mol. Biol.*, 2002, **322**, 841–849.
64 R. B. Best, S. B. Fowler, J. L. T. Herrera, A. Steward, E. Paci and J. Clarke, *J. Mol. Biol.*, 2003, **330**, 867–877.
65 I. Schwaiger, M. Schleicher, A. A. Noegel and M. Rief, *EMBO reports*, 2005, **6**, 46–51.
66 I. Schwaiger, A. Kardinal, M. Schleicher, A. A. Noegel and M. Rief, *Nat. Struct. Mol. Biol.*, 2004, **11**, 81.
67 J. Frantz, *URL: http://www.frantz.fi/software/g3data.php/ Version 1*, 2009.
68 M. Sikora, J. I. Sułkowska and M. Cieplak, *PLOS Comput. Biol.*, 2009, **5**, e1000547.
69 M. Kouza, C.-K. Hu, H. Zung and M. S. Li, *J. Chem. Phys.*, 2009, **131**, 12B608.
70 N. A. van Nuland, I. W. Hangyi, R. C. van Schaik, H. J. Berendsen, W. F. van Gunsteren, R. M. Scheek and G. T. Robillard, *J. Mol. Biol.*, 1994, **237**, 544–559.
71 A. M. Gronenborn, D. R. Filpula, N. Z. Essig, A. Achari, M. Whitlow, P. T. Wingfield and G. M. Clore, *Science*, 1991, **253**, 657–661.
72 V. Munoz, P. A. Thompson, J. Hofrichter and W. A. Eaton, *Nature*, 1997, **390**, 196–199.
73 J. Kubelka, J. Hofrichter and W. A. Eaton, *Curr. Opin. Struct. Biol.*, 2004, **14**, 76–88.
74 P. H. Nguyen, G. Stock, E. Mittag, C. K. Hu and M. S. Li, *Proteins*, 2005, **61**, 795–808.
75 B. Zagrovic, E. J. Sorin and V. Pande, *J. Mol. Biol.*, 2001, **313**, 151–169.
76 A. E. Garcia and K. Y. Sanbonmatsu, *Proteins*, 2001, **42**, 345–354.